JACS
JOURNAL OF THE AMERICAN CHEMICAL SOCIETY
Article
pubs.acs.org/JACS

High-Pressure Synthesis, Crystal Structure, and Phase Stability Relations of a $LiNbO_3$-Type Polar Titanate $ZnTiO_3$ and Its Reinforced Polarity by the Second-Order Jahn–Teller Effect

Yoshiyuki Inaguma,*[,†] Akihisa Aimi,[†] Yuichi Shirako,[†] Daichi Sakurai,[†] Daisuke Mori,[†] Hiroshi Kojitani,[†] Masaki Akaogi,[†] and Masanobu Nakayama[⊥]

[†]Department of Chemistry, Faculty of Science, Gakushuin University, 1-5-1 Mejiro, Toshima-ku, Tokyo, 171-8588, Japan

[⊥]Department of Materials Science and Engineering, Graduate School of Engineering, Nagoya Institute of Technology, Gokiso-cho, Showa-ku, Nagoya, 466-8555, Japan

Supporting Information

ABSTRACT: A polar $LiNbO_3$-type (LN-type) titanate $ZnTiO_3$ has been successfully synthesized using ilmenite-type (IL-type) $ZnTiO_3$ under high pressure and high temperature. The first principles calculation indicates that LN-type $ZnTiO_3$ is a metastable phase obtained by the transformation in the decompression process from the perovskite-type phase, which is stable at high pressure and high temperature. The Rietveld structural refinement using synchrotron powder X-ray diffraction data reveals that LN-type $ZnTiO_3$ crystallizes into a hexagonal structure with a polar space group $R3c$ and exhibits greater intradistortion of the TiO_6 octahedron in LN-type $ZnTiO_3$ than that of the SnO_6 octahedron in LN-type $ZnSnO_3$. The estimated spontaneous polarization (75 $\mu C/cm^2$, 88 $\mu C/cm^2$) using the nominal charge and the Born effective charge (BEC) derived from density functional perturbation theory, respectively, are greater than those of $ZnSnO_3$ (59 $\mu C/cm^2$, 65 $\mu C/cm^2$), which is strongly attributed to the great displacement of Ti from the centrosymmetric position along the c-axis and the fact that the BEC of Ti (+6.1) is greater than that of Sn (+4.1). Furthermore, the spontaneous polarization of LN-type $ZnTiO_3$ is greater than that of $LiNbO_3$ (62 $\mu C/cm^2$, 76 $\mu C/cm^2$), indicating that LN-type $ZnTiO_3$, like $LiNbO_3$, is a candidate ferroelectric material with high performance. The second harmonic generation (SHG) response of LN-type $ZnTiO_3$ is 24 times greater than that of LN-type $ZnSnO_3$. The findings indicate that the intraoctahedral distortion, spontaneous polarization, and the accompanying SHG response are caused by the stabilization of the polar $LiNbO_3$-type structure and reinforced by the second-order Jahn–Teller effect attributable to the orbital interaction between oxygen ions and d^0 ions such as Ti^{4+}.

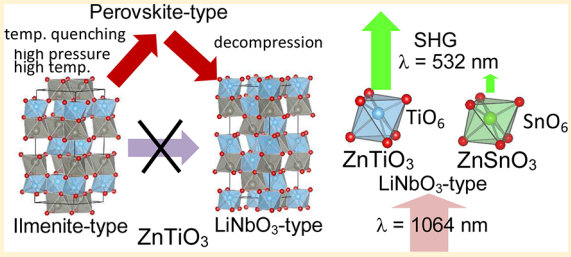

INTRODUCTION

Ferroelectricity, piezoelectricity, pyroelectricity, and second-order nonlinear optical behavior are technologically important and have been interesting topics in material science and engineering. Because these properties are attributable to the noncentrosymmetric (NCS) structure,[1] the search for materials exhibiting such characteristics must begin with a search of NCS materials. In searching for NCS materials, much attention has been paid to oxides containing second-order Jahn–Teller (SOJT) active cations,[1−10] such as d^0 transition metal ions (V^{5+}, Ti^{4+}, Nb^{5+}, Ta^{5+}, Mo^{6+}, W^{6+}, etc.) and cations with a lone pair electrons of ns^2 (Pb^{2+}, Bi^{3+} etc.). In particular, since ferroelectric perovskite-type oxides (ABO_3) containing Pb^{2+} and Bi^{3+} as A-site ions exhibit high polarization and piezoelectric performance, the new Pb- and Bi-based perovskites[11−28] have lately attracted considerable attention as candidate ferroelectric and multiferroic oxides. On the other hand, there are also naturally occurring NSC structures such as the $LiNbO_3$-type (LN-type) structure. The LN-type structure can be described as a derivative of the perovskite-type (Pv-type) structure,[29] because both LN-type and Pv-type compounds (general formula: ABX_3) possess three-dimensionally corner-sharing BX_6 octahedra. The cooperative cation shift along the hexagonal c-direction (corresponding to the 111 direction in the pseudocubic lattice of perovskite) against close-packed anions, e.g. the oxygen layer, results in spontaneous polarization. To the best of our knowledge, however, studies on functional LN-type oxides relative to Pv-type oxides have been limited because, with the exception of the well-known cases of $LiNbO_3$[30,31] and $LiTaO_3$,[32,33] only a few LN-type compounds, such as $LiUO_3$,[34−36] $LiReO_3$,[37] $Li_{1-x}Cu_xNbO_3$,[38] (Li,Cu)-TaO_3,[39] have been synthesized under ambient conditions. In contrast, in the field of earth science and high-pressure science, LN-type compounds are considered to be retrograde products of high-pressure perovskite-phases during decompression,[29] and several LN-type oxides, such as $MnMO_3$ (M = Ti,[40−43] Sn[44,45]), $FeMO_3$ (M = Ti,[41,45−47] Ge[48]), $MgMO_3$ (M = Ti,[49]

Received: August 29, 2013
Published: November 26, 2013

   dx.doi.org/10.1021/ja408931v | J. Am. Chem. Soc. 2014, 136, 2748−2756

Ge[41,50,51]), $ZnGeO_3$,[51,52] the phase close to (Ca,Mg,Fe)-Al_2SiO_6,[53] $CuTaO_3$[54] have been reported as metastable quenched phases. Among them, Sleight et al.[54] and Syono et al.[40,44] were the first to focus on the high-pressure synthesis of $LiNbO_3$-type oxides as functional materials. Following them, it has recently been reported that novel LN-type oxides, such as $ZnSnO_3$,[55−58] $CdPbO_3$,[57] $PbNiO_3$,[57,59] $(In_{1-x}M_x)MO_3$ ($x \approx 0.111-0.176$; M = $Fe_{0.5}Mn_{0.5}$),[60,61] $GaFeO_3$,[62] and $LiOsO_3$[63] synthesized under high pressure and high temperature exhibit polar structures with a hexagonal polar space group $R3c$. In addition, LN-type oxides containing transition metal ions,[64] such as $FeTiO_3$[65] and $MnMO_3$(M = Ti, Sn),[66] show the dielectric and magnetic coupling behavior and have been examined as multiferroics. These findings suggest that we might find attractive functional properties by the selection of constituent ions based on their having a naturally occurring polar LN-type structure. Among the LN-type oxides, $ZnSnO_3$[55] is composed of only d^{10} ions, Zn^{2+} and Sn^{4+}, without SOJT d^0 ions or stereoactive $6s^2$ ions, indicating that the polarity primarily originates from a polar LN-type structure stabilized using high pressure and temperature. This is supported by the fact that the calculated Born effective charges (BECs) for Zn and Sn are close to the nominal charges in $ZnSnO_3$[67,68] although the BEC of Nb is much greater than the nominal charge in $LiNbO_3$.[67,69] Furthermore, we found that the SHG intensities and dielectric permittivity of LN-type polar oxides with the second-order Jahn−Teller ions with d^0 electronic configuration (Ti^{4+}, Nb^{5+}, Ta^{5+}), such as $MnTiO_3$, $LiNbO_3$, and $LiTaO_3$, are greater than those of LN-type stannates such as $MnSnO_3$ and $ZnSnO_3$.[58] This is attributable to the high electronic polarization of SOJT active ions. On the basis of these findings, the LN-type $ZnTiO_3$ with a SOJT active ion, Ti^{4+}, is found to be one of the candidate polar oxides exhibiting high polarization. According to previous reports,[45,57] when the tolerance factor of perovskite, t, calculated using the ionic radii after Shannon[70] in an 8-fold and a 6-fold coordination for the A-site and B-site, respectively, is not more than 0.85, the LN-type phase generally appears, although there are some exceptions. The tolerance factor of $ZnTiO_3$ is 0.81, indicating that the LN-type phase is likely to appear. However, LN-type $ZnTiO_3$ has not been reported yet. Ito et al.[41] have reported that ilmenite-type (IL-type) $ZnTiO_3$ decomposes into rocksalt-type ZnO and dense fluorite-related TiO_2 (probably baddeleyite-type TiO_2[71]) at a pressure between 20 and 25 GPa. In this study, based on the report by Ito et al.,[41] we have successfully synthesized the LN-type $ZnTiO_3$ under a pressure less than 20 GPa and elucidated the crystal structure, high-pressure phase stability, and polar property, i.e., SHG response. The phase stability and the polarity were also evaluated by first principles calculation. The SOJT effect on the crystal structure and related polarity are discussed.

EXPERIMENTAL PROCEDURES

Polycrystalline $ZnTiO_3$ was synthesized by a solid-state reaction. First, the IL-type $ZnTiO_3$ was synthesized using the starting materials, wurtzite-type ZnO (>99.9% in purity) and rutile-type TiO_2 (>99.9% in purity). The metal content of the reagent of ZnO was checked by chelatometry with ethylenediaminetetraacetic acid (EDTA) prior to the usage. An equimolar mixture of starting materials was heated at 850 °C for 20 h twice with an intermediate grinding at ambient atmosphere, or at 1000 °C for 30 min under a pressure of 7.5 GPa using a cubic multianvil-type high-pressure and high-temperature apparatus (TRY, NAMO2001). In the high-pressure synthesis, the sample was sealed by an Au capsule. The details are described in the Supporting Information of our previous work.[55] LN-type $ZnTiO_3$ was synthesized using IL-type $ZnTiO_3$ as a precursor under high-pressure and high-temperature conditions in a high-pressure and high-temperature Kawai-type multianvil apparatus. The sample was then directly packed into a cylindrical Pt heater. The details of the cell assembly and the calibration of pressure were described in previous reports.[72,73] The IL-type phase was heated at 1100−1200 °C for 30 min under a pressure of 16−17 GPa and then was quenched to room temperature. In these pressure and temperature conditions, TiO_2 does not adopt a dense baddeleyite-type form but α-PbO_2-type form.[71] The obtained sample was ground and annealed at 400 °C for 12 h in air. The phase identification of the obtained samples was performed by the powder X-ray diffraction (XRD) method using a Rigaku RINT2100 diffractometer (graphite-monochromatized Cu Kα) in our laboratory. For the structure refinement for LN-type $ZnTiO_3$, synchrotron powder X-ray diffraction (SXRD) data at room temperature were collected on a Debye−Scherrer-type powder diffractometer with an imaging plate-type detector installed at the BL02B2 beamline at SPring-8.[74] The scan step size was 0.01° in 2θ at a wavelength of λ = 0.42030 Å for LN-type $ZnTiO_3$. Here, the sample was packed into a glass capillary of 0.2 mm diameter. The crystal structure was refined using the Rietveld analysis program, *RIETAN-FP*.[75] The crystal structures were drawn using the program *VESTA*[76] based on the structural refinement results. Powder second harmonic generation (SHG) measurements at room temperature were performed on a modified Kurtz[77] nonlinear optical system using 1064 nm light. The ungraded polycrystalline LN-type $ZnTiO_3$ was used for measurement of the SHG response. Due to the small amount of sample, we could not check the particle size-dependence of the SHG signal. To make relevant comparisons with known SHG materials, $LiNbO_3$ powders were also prepared. The SHG radiation was collected in reflection mode using a Continuum Minilite II YAG:Nd laser (λ = 1064 nm) operating at 10 Hz. The reflected radiation from the sample, after passing an IR cutoff filter to remove the incident laser light, was introduced into a monochromator (MC-10N; Ritu Co., Ltd.) using an optical fiber in order to extract only the radiation with a wavelength of 532 nm, and detected by an attached photomultiplier tube (PMT) (R6427; Hamamatsu Photonics). A digital oscilloscope (RTM1052; Rohde and Schwarz) connected with the PMT via a preamplifier was used in order to monitor and collect the SHG data. The intensity of incident laser light was checked by a photodiode behind an ND filter. The phase stabilities of three $ZnTiO_3$ compounds with LN-type, IL-type, and Pv-type structures were evaluated by first principles density functional theory (DFT). Vienna *ab initio* simulation package (VASP) ver. 5.2[78,79] was utilized with the modified Perdew−Burke−Ernzerhof generalized gradient approximation (PBEsol-GGA)[80,81] and with the projector-augmented wave (PAW) method.[82] Spin polarization calculation was adopted. Relaxation was allowed and the final energies of the optimized geometries were recalculated so as to correct for changes in the plane-wave basis during relaxation. A kinetic cutoff energy of 500 eV was found by a convergence test (<3 meV/LN-type $ZnTiO_3$). Relaxed structure calculations were performed at various constant volumes, and then the energy-volume data were fitted to the Murnaghan equation of state[83]

$$E(V) = B_0V_0\left[\frac{1}{B'(B'-1)}\left(\frac{V_0}{V}\right)^{B'-1} + \frac{V}{B'V_0} - \frac{1}{(B'-1)}\right] + E_0 \quad (1)$$

where B_0 is the bulk modulus at zero pressure, B' its first derivative, E_0 the minimum energy, and V_0 the volume at the minimum energy. In addition, the original definition of bulk modulus B can be expressed as follows:

$$B = -V\,dp/dV \quad (2)$$

where V and p are volume and pressure, respectively. By combining eqs 1 and 2, we obtained an enthalpy-pressure diagram for the calculated structures. Phonon frequencies and their contribution to free energy changes were calculated by the supercell approach using PHONOPY code.[84] Density functional perturbation theory (DFPT),[85]

dx.doi.org/10.1021/ja408931v | J. Am. Chem. Soc. 2014, 136, 2748−2756

also implemented in VASP, was used to estimate the real-space force constants of supercells.

RESULTS AND DISCUSSION

Phase identification, structure refinement of $LiNbO_3$-type $ZnTiO_3$. The X-ray diffraction (XRD) patterns for ilmenite-type (IL-type) $ZnTiO_3$ synthesized using two different processes are shown in Figure S1 of the Supporting Information [SI]. The IL-type phase is in accordance with the phase in the previous report.[86] When IL-type $ZnTiO_3$ was synthesized at ambient pressure, a small amount of spinel-type Zn_2TiO_4 and rutile-type TiO_2 as impurity phases were observed, while the single phase of IL-type $ZnTiO_3$ was obtained by high-pressure synthesis. The sample recovered after the heat treatment of IL-type $ZnTiO_3$ at 1200 °C for 30 min under a pressure of 16 GPa exhibited a bluish-gray color attributable to a small amount of oxygen vacancies. The sample after annealing at 400 °C for 12 h in air exhibited the same X-ray diffraction pattern as the pristine sample, although the color changed to light gray. As seen in Figure 1, the powder XRD

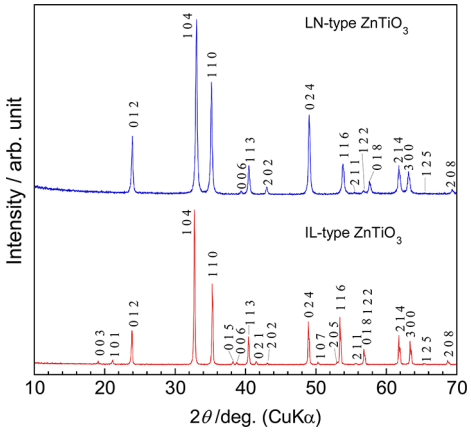

Figure 1. Powder X-ray diffraction patterns for $LiNbO_3$ (LN)-type and ilmenite (IL)-type $ZnTiO_3$.

pattern of the sample was different from that of IL-type $ZnTiO_3$ (space group: $R\bar{3}$ (No. 148)), although the diffraction peaks could be indexed under the assumption of a hexagonal lattice. It can be easily recognized that diffraction peaks with mirror indices, such as 0 0 3 and 1 0 1, are absent, indicating that their space group is different from that of IL-type $ZnTiO_3$ and that phase transformation from the IL-type phase occurred. In addition, the sample exhibited positive SHG response indicating NCS, while the centrosymmetric IL-type phase showed no SHG response. Considering the reflection condition of the XRD pattern ($-h + k + l = 3n$ for $hkil$, $l = 2n$ for $h-h0l$, and $l = 6n$ for $000l$ (n: integer)) and positive SHG response, the sample possesses a hexagonal polar space group $R3c$ (No. 161) just as LN-type $ZnSnO_3$ does. The Rietveld structure refinement using SXRD data based on the findings ensured that the sample possesses an LN-type structure with $R3c$. Figure 2 displays the observed and calculated SXRD patterns and their differences for LN-type $ZnTiO_3$ (annealed sample at 400 °C, 12 h in air) at room temperature. The refined structural parameters for LN-type $ZnTiO_3$ are listed in Table 1. The selected interatomic distances and the bond angles of LN-type $ZnTiO_3$ are also listed in Table S1 of the SI. The calculation of bond valence sum (BVS)[87−90] using the interatomic distances shown in SI, Table S1, gives 1.98 for Zn and 4.01 for Ti. These

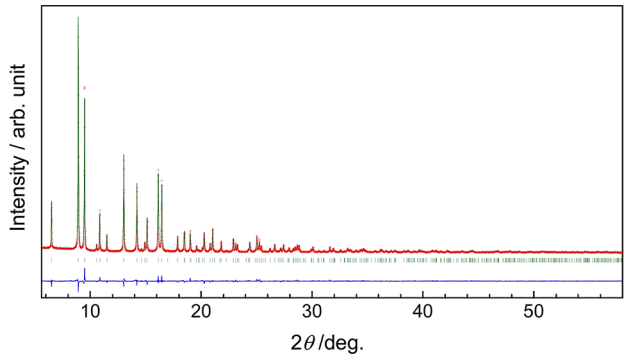

Figure 2. Observed (+) and calculated (solid line) powder synchrotron X-ray diffraction patterns, difference (solid line on the bottom), and peak positions (|) for $LiNbO_3$-type $ZnTiO_3$ at room temperature.

Table 1. Structural Parameters for $LiNbO_3$-Type $ZnTiO_3$ at Room Temperature[a]

atom	site	x	y	z	B/Å^2
Zn	6*a*	0	0	0.27913(5)	0.825(18)
Ti	6*a*	0	0	0	0.134(17)
O	18*b*	0.0403(4)	0.3386(3)	0.06378(17)	0.547(3)

[a]Hexagonal, space group $R3c$ (No. 161), $Z = 6$, $a = 5.09452(12)$ Å and $c = 13.7177(3)$ Å, $V = 308.332(12)$ Å^3; $R_{wp} = 3.36\%$, $R_p = 2.54\%$, $R_e = 3.63\%$, $S = 0.93$, $R_B = 2.15\%$, $R_F = 1.86\%$

values are consistent with the nominal ones. Figure 3 shows the refined crystal structures of IL-type and LN-type $ZnTiO_3$. As

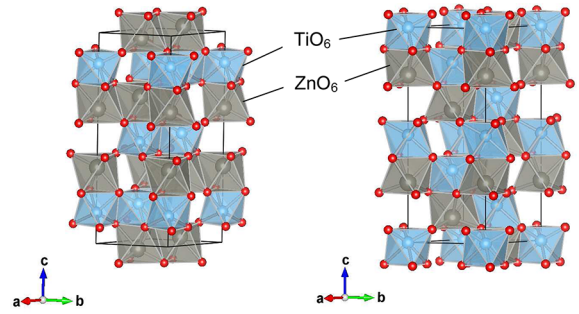

(a) Ilmenite-type (b) $LiNbO_3$-type

Figure 3. Crystal structures of ilmenite-type $ZnTiO_3$ (a) and $LiNbO_3$-type $ZnTiO_3$ (b).

shown in Figure 3, between IL-type and LN-type $ZnTiO_3$, the stacking of BO_6 octahedra is different. In ilmenite-type oxides, the AO_6 and BO_6 octahedra are linked with shared edges, and the A and B ions are alternatively stacked along the c-axis. On the other hand, in $LiNbO_3$-type oxides, the BO_6 octahedra are linked with shared corners just as in perovskite-type oxides. Therefore, from ilmenite to lithium niobate or perovskite, cation rearrangement is required. Furthermore, attributable to the difference in the stacking, the cation−cation repulsion between A and B ions in ilmenite-type structure directs the cancellation of polarization, on the other hand, the cation−cation repulsion in $LiNbO_3$-type structure directs the polarization along c-axis.

Phase Stability Relations of $ZnTiO_3$ Polymorphs. The lattice volume of LN-type $ZnTiO_3$ (51.4 Å^3/ f.u.) is smaller

dx.doi.org/10.1021/ja408931v | J. Am. Chem. Soc. 2014, 136, 2748−2756

than that of the IL-type phase (51.9 Å^3/f.u.),[86] which is consistent with the fact that the LN-type phase was obtained by high-pressure synthesis. The lattice volume of LN-type $ZnTiO_3$ is much greater than the sum (45.8 Å^3/f.u.) of the lattice volumes of NaCl-type ZnO[91] and baddeleyite-type TiO_2,[71] indicating that in the pressure region more than 20 GPa $ZnTiO_3$ decomposes into ZnO and TiO_2, as Ito et al. have reported.[41] On the other hand, the lattice volume of LN-type $ZnTiO_3$ (51.4 Å^3/ f.u.) is slightly greater than the sum (50.3 Å^3/f.u.) of the lattice volumes of NaCl-type ZnO[91] and α-PbO_2-type TiO_2,[92] which are thought to be stable at 16−17 GPa, respectively. This finding suggests the presence of a compound more dense than LN-type $ZnTiO_3$, with a smaller lattice volume than the sum of those of NaCl-type ZnO[91] and α-PbO_2-type TiO_2.[92] As mentioned above, in the field of earth science, the LN-type phases are considered to be retrograde products of high-pressure perovskite-phases during decompression. The Pv-type $ZnTiO_3$ is probably stable at 16−17 GPa and transforms to the LN-type phase in the decompression process. The phase stability was then evaluated by first principles calculation. Table 2 lists the optimized crystal structures of LN-type $ZnTiO_3$. The results show good accordance with the experimental ones shown in Table 1. Figure 4 displays the variation of the total energy for LN-type $ZnTiO_3$ as a function of cell volume. The solid line in the figure represents the fitted line using the Murnaghan equation of state, and shows good fits ranging from ∼80 to ∼110 vol % against the ground-state structure. In the same way, fitting was carried out for the IL-type and Pv- type $ZnTiO_3$ compounds. Note that the initial lattice and ion configurations of the Pv-type $ZnTiO_3$ refer to the reported structure of $CaTiO_3$ with *Pnma* symmetry.[93] The fitting results, the cell volume V_0, and the bulk modulus B_0 at zero pressure, are summarized in Table 3. The volume of the LN-type phase is smaller than that of the IL-type phase, that of the Pv-type phase is smaller than those of the other two phases, and the Pv-type phase becomes the most stable phase at a volume region smaller than around 44 Å^3/f.u. Hence, the Pv-type structure is expected to be stable at a high-pressure region. Furthermore, the calculated lattice volume of Pv-type $ZnTiO_3$ (49.7 Å^3/f.u.) is slightly smaller than the sum (50.3 Å^3/f.u.) of the lattice volumes of the NaCl-type ZnO[91] and α-PbO_2-type TiO_2,[92] which supports the notion that Pv-type $ZnTiO_3$ is stable at 16−17 GPa. Using eq 2 relationship, the pressure dependences of the enthalpy ($E + pV$) for three types of $ZnTiO_3$ phase were plotted as a solid line in Figure 5a. The enthalpy of LN-type was set as zero for purposes of comparison (relative enthalpy), and zero-point energy correction and the phonon contribution were not included. In the pressure range below 25 GPa, the IL-type phase is the most stable in terms of enthalpy, indicating that the LN-type $ZnTiO_3$ never appears by increasing pressure. The relative enthalpy or free energy of the Pv-type phase decreases more rapidly with pressure than that of the IL-type phases because this phase has a smaller volume than the other structures. The calculated phonon-dispersion curves of LN-type $ZnTiO_3$ are presented in the SI, Figure S2. The absence of imaginary frequencies indicates that the LN-type $ZnTiO_3$ phase is a dynamically stable structure. By considering the phonon contribution, the free energy (relative free energy) at 1200 °C as a function of pressure was also plotted as the hatched line in Figure 5a. As seen in the figure, the relative free energies of the Pv-type and IL-type phases decreased and increased with the temperature increase, respectively. As a result, the Pv-type phase formed thermodynamically above 13.5 GPa, while the LN-type phase could not be stabilized. We confirmed that the LN-type phase is always thermodynamically unstable among the three polymorphs within the computed range of temperature (<1500 °C) and pressure (<25 GPa). The thermodynamical instability at any pressure and temperature of LN-type $ZiTiO_3$ under the present computations was obviously inconsistent with the formation of LN-type $ZnTiO_3$ in the present experiments. We infer that kinetic effects suppress the phase transition from Pv-type to IL-type $ZnTiO_3$, but allow that from the Pv-type to LN-type phase by reducing the pressure at room temperature. As mentioned above, the arrangements of ions in the Pv-type and the LN-type structures are topologically equivalent, where both the Pv-type and LN-type structures consist of a framework of corner-sharing octahedra containing Ti (TiO_6), and Zn ions are located inside the framework. Hence, diffusionless transformation is conceivable between two structures even at relatively low temperature. This is supported by the fact that Pv-type $PbNiO_3$ is transformed to LN-type $PbNiO_3$ at 250 °C at ambient pressure.[59] On the other hand, the crystal structure of IL-type $ZnTiO_3$, where each TiO_6 octahedron shares three edges with adjacent octahedra, forming

Table 2. Structure Parameters for LN-Type $ZnTiO_3$ Obtained by First Principles DFT Calculation

atom	site	*x*	*y*	*z*
Calculation[a]				
Zn	6*a*	0	0	0.2814
Ti	6*a*	0	0	0[b]
O	18*b*	0.0441	0.3454	0.0653

[a]Hexagonal, space group *R3c* (No. 161), $Z = 6$, $a = 5.0875$ Å and $c = 13.7160$ Å. [b]The fractional *z* coordinate for Ti was fixed to be zero.

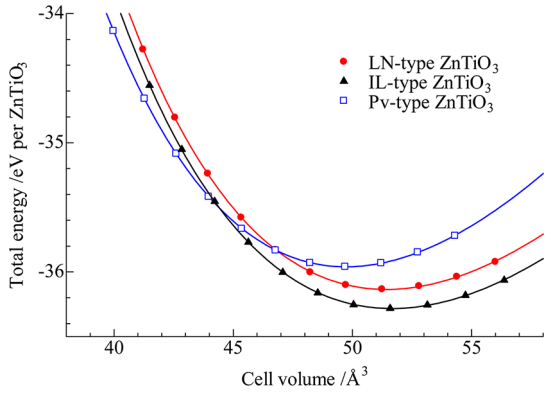

Figure 4. (a) The variation of total energy as a function of cell volume for LN-type, Pv-type, and IL-type $ZnTiO_3$. The solid line is a fitted line using the Murnaghan equation of state.[83]

Table 3. List of the Volumes and Bulk Moduli at Zero Pressure for Various $ZnTiO_3$ Polymorphs Calculated by First-Principles DFT ('f.u.' = formula units)

cmpds	volume/Å^3 f.u.	bulk modulus/GPa
IL-type $ZnTiO_3$	51.6	191
LN-type $ZnTiO_3$	51.2	204
Pv-type $ZnTiO_3$	49.7	214

dx.doi.org/10.1021/ja408931v | J. Am. Chem. Soc. 2014, 136, 2748−2756

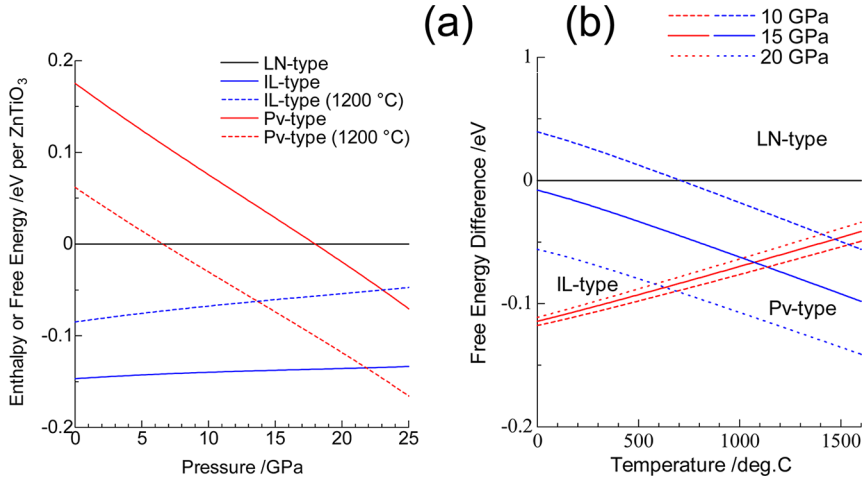

Figure 5. (a) Pressure dependence of the relative enthalpies or free energies for three types of $ZnTiO_3$ phases. The solid line corresponds to the enthalpy without a temperature effect and zero-point energy correction, whereas the hatched line represents the free energy at 1200 °C. The energy of LN-type $ZnTiO_3$ is set as zero for purposes of comparison. (b) Temperature dependence of the relative free energies for three $ZnTiO_3$ phases.

two-dimensional TiO_6 sheets, is not topologically consistent with the others, indicating that the phase transition from Pv-type to IL-type is unlikely in terms of kinetics at the low temperature region. Figure 5b presents relative free energies of the three types of $ZnTiO_3$ polymorphs as a function of temperature at various pressures. The phase transition temperature from the IL-type to Pv-type $ZnTiO_3$ phase (IL→Pv phase transition) decreases by increasing pressure, i.e., the ilmenite−perovskite phase boundaries have negative slopes and are expressed as $P(\mathrm{GPa}) = 29.1 - 0.0105T$ (K), indicating that the entropy of the Pv-type phase is greater than that of the IL-type phase. This is the common feature in the phase transition between the Pv-type and IL-type phases.[29] On the other hand, the phase transition from Pv-type to LN-type $ZnTiO_3$ (Pv→LN phase transition) driven by a diffusionless mechanism occurs at a lower temperature than the Pv→IL phase transition, and the Pv→LN phase transition temperature decreases with increasing pressure. Therefore, we interpret the experimental synthesis of the LN-type $ZnTiO_3$ phase as follows: (i) The Pv-type $ZnTiO_3$ was formed under a high-pressure and high-temperature conditions. (ii) By temperature quenching, the Pv-type structure remained without the transformation to IL-type phase, although the IL-phase is thermodynamically more stable than the Pv-phase at intermediate temperature. (In this temperature region, the LN-type phase is unstable against both of the IL- and Pv-phases.) The temperature-quenching process kinetically inhibited the rearrangement of ionic configuration between IL- and Pv-type structures. (iii) The LN-type phase appeared due to the diffusionless Pv→LN phase transition in the decompression process at room temperature (in the case of 10−15 GPa in Figure 5b). With respect to process (i), the experimental finding that LN-type $ZnTiO_3$ was obtained under the conditions of 16 GPa and 1200 °C was consistent with the calculation result that under this condition the Pv-phase is stable, as seen in Figure 5b. Furthermore, it is worth noting that the suppression of the Pv→IL phase transition in process (ii) could be ascribed to the kinetic effect, as mentioned above. In fact, when LN-type $ZnTiO_3$ was annealed at 500 °C for 12 h in air, a transformation to the IL-type phase occurred. The experimental details of the pressure−temperature phase relation of $ZnTiO_3$ will be reported in the near future.

Relationship between the Crystal Structure, Electronic Properties and Polarity of $LiNbO_3$-Type $ZnTiO_3$ and Other Oxides. The ionic polarization, P_s, was calculated by use of a simple point-charge model and is given by

$$P_s = \left(\sum_i q_i \delta d_i\right)/V \tag{3}$$

where V is the unit-cell volume, q_i is the nominal charge on the ith atom and δd_i is the displacement along the c-axis of the ith atom from its position in the centrosymmetric structural arrangement in which $P_s = 0$. The calculated polarization is 75 $\mu C/cm^2$, which is greater than those of $ZnSnO_3$ (59 $\mu C/cm^2$)[55] and $LiNbO_3$ (62 $\mu C/cm^2$).[94] Next, we estimate the intra-distortion of the BO_6 octahedron, Δ_B, which is defined by the following equation.[87] Here, d_i is the interatomic distance and d_{AV} is the average of the interatomic distances.

$$\Delta_B = 1/6 \sum_{i=1}^{6} \{(d_i - d_{AV})/d_{AV}\}^2 \tag{4}$$

The Δ_B for TiO_6 in LN-$ZnTiO_3$ is 47×10^{-4}, which is 1 order of magnitude greater than the Δ_B of SnO_6 in LN-$ZnSnO_3$,[55] 5×10^{-4}, and is close to the value of 40×10^{-4} for NbO_6 in $LiNbO_3$.[94] The shifts of A-site and B-site ions from their centrosymmetric positions (fractional coordinates), δz_A and δz_B, calculated spontaneous polarizations, P_s, and intra-octahedral distortions of BO_6, Δ_B for LN-type $ZnTiO_3$, $ZnSnO_3$, and $LiNbO_3$, are summarized in Table 4. Note that the displacements of Zn and Ti ions are estimated by assuming corresponding centrosymmetric structures with $R\,\bar{3}\,c$ symmetry, in which the A and B ions are located in the center of the oxygen triangle plane and the center of the BO_6 oxygen octahedral cages, respectively.[69] As seen in Table 4, δz_B in

Table 4. Structural Parameters and Polarization for $LiNbO_3$-Type $ZnTiO_3$, $ZnSnO_3$, and $LiNbO_3$ at Room Temperature

cmpds	δz_A	δz_B	P_s /μCcm^{-2}	Δ_B
$ZnTiO_3$	0.0487	0.0196	75	47×10^{-4}
$ZnSnO_3$	0.0483	0.0124	59	5×10^{-4}
$LiNbO_3$	0.0487	0.0200	62	40×10^{-4}

dx.doi.org/10.1021/ja408931v | J. Am. Chem. Soc. 2014, 136, 2748−2756

$ZnTiO_3$ and $LiNbO_3$ is much greater than that in $ZnSnO_3$, though the values of δz_A are close, indicating that the greater polarization in $ZnTiO_3$ and $LiNbO_3$ than in $ZnSnO_3$ is primarily attributable to the large shift of Ti/Nb ions. The greater shifts and intraoctahederal distortions of BO_6 in $ZnTiO_3$ and $LiNbO_3$ are likely attributable to an SOJT effect based on the hybridization between the empty Ti 3d/Nb $4d_\pi(t_{2g})$ orbital (LUMO) and occupied O $2p_\pi$ orbital (HOMO). The variation of Δ_B versus δz_B for various $LiNbO_3$-type oxides is plotted in Figure 6. Here, we calculated the values of Δ_B and δz_B for other

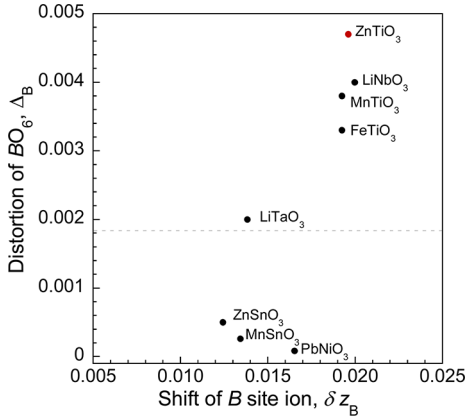

Figure 6. Variation in the distortion of the BO_6 octahedron, Δ_B versus the shift of the B-site ion from the centro-symmetric position, and δz_B for various $LiNbO_3$-type oxides.

compounds than $ZnTiO_3$, $LiNbO_3$, and $ZnSnO_3$ shown in Table 4 using the reported structural parameters. We then adopted the structural parameters in previous reports on $MnMO_3$ (M = Ti, Sn),[66] $FeTiO_3$,[47] $LiTaO_3$,[32] and $PbNiO_3$.[59] The magnitude of Δ_B does not necessarily increase with δz_B, though such a tendency can be seen. On the other hand, it is noteworthy that the Δ_B for the compound with d^0 B ions such as Ti^{4+}, Nb^{5+}, and Ta^{5+}, is much greater than that for stanates and nickelate. These data indicate that the distortion of BO_6 in $LiNbO_3$-type oxides with d^0 B ions is effectively brought about by the SOJT effect. Furthermore, the order of Δ_B among the compounds with d^0 B ions is as follows: Ti^{4+}, $Nb^{5+} > Ta^{5+}$. The SOJT distortions occur when a HOMO−LUMO energy gap is sufficiently small and there is a symmetry-allowed distortion giving rise to mixing between the two orbitals. Wheeler and Hoffmann et al.[7] and Kunz and Brown[8] pointed out that, when the B ion is a d^0 ion, the magnitude of the intradistortion of BO_6 attributable to the SOJT effect depends inversely on the energy gap between the empty $d_\pi(t_{2g})$ orbital (LUMO) and occupied oxygen 2p orbital (HOMO). From the difference in electronegativity[95] between these SOJT ions and oxygen, we can expect the energy gap to be $Zr^{4+} > Ta^{5+} > Nb^{5+} > Ti^{4+}$. Furthermore, we can infer that the energy gap correlates to the band gap energy because the top of valence band is primarily derived from O 2p nonbonding, and the conduction band is primarily contributed by the antibonding B $d(t_{2g})$-O $2p\pi^*$ orbital in the compounds with corner-shared BO_6 octahedra such as perovskite-type and $LiNbO_3$-type oxides. In fact, the experimental optical band gap energies of perovskite-type for AMO_3 (M = Ti^{4+}, Nb^{5+}, Ta^{5+})[96,97] are 3.1 eV for $SrTiO_3$, 3.4 eV for $CaTiO_3$, 3.1 eV for $KNbO_3$, 3.4 eV for $NaNbO_3$, 3.2 eV for $La_{1/3}NbO_3$, 3.5 eV for $KTaO_3$, 4.0 eV for $NaTaO_3$, 3.9 eV for $La_{1/3}TaO_3$. Summarizing these data, the optical band gap energies are the following order: $Ta^{5+} > Ti^{4+}$, Nb^{5+}. From the consideration of electronegativity and band gap energy, we can expect the order of magnitude of the SOJT effect to be Ti^{4+}, $Nb^{5+} > Ta^{5+}$, which is consistent with the results seen in Figure 6. These findings are further supported by the intradistortion of the BO_6 octahedron calculated from the structure parameters by first principles DFT calculation, Δ_{BFP} and the Born effective (dynamic) charge (BEC). The BEC tensors of the LN-type $ZnTiO_3$ and spontaneous polarization along the c-axis were calculated using the DFPT approach (Table 5).[85] For the

Table 5. List of Averaged Diagonal Components of Born Effective Charge (BEC) Tensors, Δ_{BFP} and Spontaneous Polarization, p, along the c-Axis for LN-Type $ZnMO_3$ (M = Sn, Ge, Ti, Zr) and $LiNbO_3$ Obtained by First Principles DFT Calculation[a]

	BEC				
cmpds	Zn or Li	M or Nb	Δ_{BFP}	p /μC cm^{-2}	$I_{A/B}$
$ZnTiO_3$	2.35	6.14	27×10^{-4}	88.1	1.1
$ZnGeO_3$	2.27	4.33	5×10^{-4}	60.4	1.8
$ZnZrO_3$	2.33	5.84	4×10^{-4}	78.1	1.2
$ZnSnO_3$	2.32	4.12	2×10^{-4}	65.2	1.7
$LiNbO_3$	1.15	7.19	22×10^{-4}	75.8	0.4

[a] $I_{A/B}$ refers to the contribution of cation displacements at two sites to the spontaneous polarization, p (see main text).

purposes of comparison, the calculations were also performed for the isostructural compounds of $ZnMO_3$ (M = Ge, Zr, Sn) and $LiNbO_3$. Among them, only $ZnZrO_3$ is a virtual compound. The lattice parameters and fractional coordinates of ions obtained by the DFT calculations are given in the SI, Table S-2. The calculated intradistortion of the BO_6 octahedron, Δ_{BFP} of $ZnTiO_3$ and $LiNbO_3$ with d^0 B ion, is greater than that of $ZnGeO_3$ and $ZnSnO_3$, while the Δ_{BFP} of $ZnZrO_3$ is almost the same, although the Zr^{4+} ion has a d^0 electronic configuration. This is partly attributable to the difference in energy gap for the compound with d^0 B ions, $Zr^{4+} > Ta^{5+} > Ti^{4+}$, Nb^{5+}. Among the computed compounds, $ZnTiO_3$, which was synthesized in this study, showed the largest spontaneous polarization of 88.0 μC/cm^2. The finding that the polarization of $ZnTiO_3$ was greater than that of $ZnSnO_3$ is consistent with the experimental results. This was due to the difference in the BEC between Ti (∼+6.1) and Sn (∼+4.1), as listed in Table 5. As stated above, the BEC of Zr (∼+5.8) in the $ZnZrO_3$ phase and of Nb (∼+7.2) in the $LiNbO_3$ phase are deviated from nominal charges (Zr^{4+} and Nb^{5+}), while that of Ge (∼+4.3) in the $ZnGeO_3$ phase showed accordance with nominal charge. The common feature of the metal ions, Ti, Zr, and Nb, which possess larger BEC than the corresponding nominal charges, is the d^0 electronic configuration, so that the SOJT mechanism can account for the deviation of the BECs. Table 5 also lists the indices that represent the contribution of ionic displacement at Zn^{2+} (Li^+) and M^{4+} (Nb^{5+}) in $ZnMO_3$ ($LiNbO_3$) compounds to the spontaneous polarization. The definition of the indices is expressed as follows,

$$I_{A/B} = p(\mathrm{Zn})/p(\mathrm{M}),\ (\mathrm{or} = p(\mathrm{Li})/p(\mathrm{Nb}) \mathrm{for}\ LiNbO_3) \quad (5)$$

where p(X) indicates the electronic polarization of the X ion calculated by considering the ionic displacement and the BEC of the X ion. The indices for $ZnSnO_3$ and $ZnGeO_3$ are larger than unity (1.7 and 1.8, respectively), so that the displacement

dx.doi.org/10.1021/ja408931v | J. Am. Chem. Soc. 2014, 136, 2748−2756

of Zn^{2+} largely affects the spontaneous polarization. On the other hand, the small index of $LiNbO_3$ (0.4) indicates the significant contribution of the ionic displacement of Nb^{5+} to the spontaneous polarization. The opposite trend between $ZnSnO_3$ or $ZnGeO_3$ and $LiNbO_3$ can be explained by the twice-larger nominal charges of Zn^{2+} than Li^+ and the SOJT effect of the Nb^{5+} ion. The indices of $ZnTiO_3$ and $ZnZrO_3$ are close to unity, and thus both effects, the divalency of the Zn ion and large BEC for the d^0 transition metal ion, result in the relatively large spontaneous polarizations. Furthermore, the calculation suggests that $ZnZrO_3$ is a candidate $LiNbO_3$-type compound.

Figure 7 shows the SHG response of LN-type $ZnTiO_3$. For comparison, the SHG response of $ZnSnO_3$ is also presented.

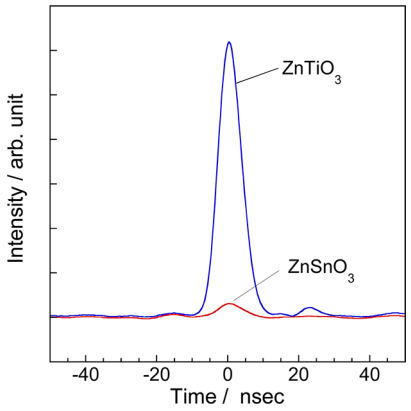

Figure 7. Comparison of SHG intensities for $LiNbO_3$-type $ZnTiO_3$ and $ZnSnO_3$.

The SHG intensity of LN-type $ZnTiO_3$ is 24 times greater than that of LN-type $ZnSnO_3$, and it corresponds to 5% of the SHG response for $LiNbO_3$. The SHG response can be explained by using the anharmonic model with the following potential.[98]

$$V(x) = \frac{m\omega_0^2}{2}x^2 + Dx^3 \tag{6}$$

Here, for simplicity, we consider a one-dimensional oscillator of the noncentrosymmetric system. D is the anharmonic potential coefficient. Using the linear electric susceptibility, $\chi(\omega)$, the second-order anharmonic susceptibility, $\chi^{(2)}(2\omega, \omega, \omega)$ is given by

$$\chi^{(2)}(2\omega; \omega, \omega) = \frac{3|D|\varepsilon_0^2}{N^2e^3}\chi(2\omega)[\chi(\omega)]^2 \tag{7}$$

When we assume that $\chi(2\omega) \approx \chi(\omega)$ and introduce the relation between the refractive index, n and $\chi(\omega)$, $n^2 = 1 + \chi(\omega)$ to eq 7, we have

$$\chi^{(2)}(2\omega; \omega, \omega) \approx \frac{3|D|\varepsilon_0^2}{N^2e^3}(n^2 - 1)^3 \tag{8}$$

The SHG intensity, I is therefore given by

$$I \propto \chi^{(2)^2} \propto D^2(n^2 - 1)^6 \tag{9}$$

From eq 9, the SHG intensity is primarily dependent on the anharmonic potential coefficient and refractive index. The much greater SHG response of $ZnTiO_3$ than that of $ZnSnO_3$ reveals that the anharmonic potential coefficient of $ZnTiO_3$ is greater than that of $ZnSnO_3$ because the refractive index of $ZnSnO_3$ is thought to be close to or greater than that of $ZnTiO_3$. The anharmonic potential coefficient is therefore enhanced by the intradistortion of BO_6 octahedra. Consequently, the polar properties such as polarization and SHG response in LN-type $ZnTiO_3$ are brought about by the stabilization of the polar $LiNbO_3$-type structure and reinforced by the SOJT effect of Ti^{4+} ion.

CONCLUSION

The polar $LiNbO_3$-type $ZnTiO_3$ was successfully synthesized under a pressure of 16−17 GPa and 1100−1200 °C. The first principles calculation indicates that LN-type $ZnTiO_3$ is a metastable phase obtained by transformation in the decompression process from perovskite-type phase stable at high temperature and high pressure. This is consistent with the experimental results. The greater polarization and SHG response in LN-type $ZnTiO_3$ compared to those in LN-type $ZnSnO_3$ are primarily attributable to the SOJT effect of the Ti^{4+} ion. We found that the distortion of BO_6 octahedra and the accompanying polar properties in LN-type oxides are brought about by the stabilization of the LN-type structure using high-pressure synthesis and reinforced by the second-order Jahn−Teller effect of the d^0 ion. This is supported by the finding that the Born effective charge (BEC) of the d^0 ion is much greater than the nominal charge. Taken together, the findings reveal that the cooperative SOJT effect in polar compounds such as $LiNbO_3$-type oxides with the d^0 B ion, e.g., $LiNbO_3$, $LiTaO_3$, $ATiO_3$ (A = Mg, Mn, Fe, Zn), $ZnZrO_3$ would result in excellent polar properties. The spontaneous polarization of LN-type $ZnTiO_3$ is greater than that of $LiNbO_3$, indicating that LN-type $ZnTiO_3$, like $LiNbO_3$, is a candidate ferroelectric material with high performance. The high-pressure synthesis of LN-type $ZnTiO_3$ suggests that epitaxial stabilization of LN-type $ZnTiO_3$ in a thin film form might be possible, as has recently been demonstrated for LN-$ZnSnO_3$.[56] The measurement of ferroelectricity of LN-type $ZnTiO_3$ in a thin film form remains a subject for future study.

ASSOCIATED CONTENT

Supporting Information

Selected interatomic distances and the bond angles of $LiNbO_3$-type $ZnTiO_3$. Structure parameters for LN-type $ZnMO_3$ (M = Ge, Zr, Sn) and $LiNbO_3$ obtained by first principles DFT calculation. XRD patterns for ilmenite-type $ZnTiO_3$. Phonon-dispersion relations of the LN-type $ZnTiO_3$. CIF of $LiNbO_3$-type $ZnTiO_3$. This material is available free of charge via the Internet at http://pubs.acs.org.

AUTHOR INFORMATION

Corresponding Author

yoshiyuki.inaguma@gakushuin.ac.jp

Notes

The authors declare no competing financial interest.

ACKNOWLEDGMENTS

We thank Mr. Takayuki Ishii and Kohei Abe for their help with the high-pressure synthesis and Prof. Koichi Iwata of Gakushuin University for his helpful advice on the optical setup for the SHG measurement. The SXRD experiment was conducted at the BL02B2 beamline at SPring-8 with the approval of JASRI (2011B1453 and 2013A1697). This work was supported by JSPS KAKENHI Grant Numbers 21360325, 24360275 and 25709059, a promotional project for the

Development of a Strategic Research Base for Private Universities, and a matching fund subsidy from the Ministry of Education, Culture, Sports, Science and Technology, Japan.

REFERENCES

(1) Halasyamani, P. S.; Poeppelmeier, K. R. *Chem. Mater.* **1998**, *10*, 2753.
(2) Opik, U.; Pryce, M. H. L. *Proc. R. Soc. London., Series A* **1957**, *238*, 425.
(3) Bader, R. F. W. *Mol. Phys.* **1960**, *3*, 137.
(4) Pearson, R. G. *J. Am. Chem. Soc.* **1969**, *91*, 4947.
(5) Pearson, R. G. *J. Mol. Struct. (THEOCHEM)* **1983**, *103*, 25.
(6) Hughbanks, T. *J. Am. Chem. Soc.* **1985**, *107*, 6851.
(7) Wheeler, R. A.; Whangbo, M. H.; Hughbanks, T.; Hoffmann, R.; Burdett, J. K.; Albright, T. A. *J. Am. Chem. Soc.* **1986**, *108*, 2222.
(8) Kunz, M.; Brown, I. D. *J. Solid State Chem.* **1995**, *115*, 395.
(9) Goodenough, J. B. *Annu. Rev. Mater. Sci.* **1998**, *28*, 1.
(10) Halasyamani, P. S. *Chem. Mater.* **2004**, *16*, 3586.
(11) Eitel, R. E.; Randall, C. A.; Shrout, T. R.; Rehrig, P. W.; Hackenberger, W.; Park, S.-E. *Jpn. J. Appl. Phys., Part 1* **2001**, *40*, 5999.
(12) Eitel, R. E.; Randall, C. A.; Shrout, T. R.; Park, S.-E. *Jpn. J. Appl. Phys., Part 1* **2002**, *41*, 2099.
(13) Shpanchenko, R. V.; Chernaya, V. V.; Tsirlin, A. A.; Chizhov, P. S.; Sklovsky, D. E.; Antipov, E. V.; Khlybov, E. P.; Pomjakushin, V.; Balagurov, A. M.; Medvedeva, J. E.; Kaul, E. E.; Geibel, C. *Chem. Mater.* **2004**, *16*, 3267.
(14) Belik, A. A.; Azuma, M.; Saito, T.; Shimakawa, Y.; Takano, M. *Chem. Mater.* **2004**, *17*, 269.
(15) Azuma, M.; Takata, K.; Saito, T.; Ishiwata, S.; Shimakawa, Y.; Takano, M. *J. Am. Chem. Soc.* **2005**, *127*, 8889.
(16) Hughes, H.; Allix, M. M. B.; Bridges, C. A.; Claridge, J. B.; Kuang, X.; Niu, H.; Taylor, S.; Song, W.; Rosseinsky, M. J. *J. Am. Chem. Soc.* **2005**, *127*, 13790.
(17) Belik, A. A.; Wuernisha, T.; Kamiyama, T.; Mori, K.; Maie, M.; Nagai, T.; Matsui, Y.; Takayama-Muromachi, E. *Chem. Mater.* **2005**, *18*, 133.
(18) Belik, A. A.; Iikubo, S.; Kodama, K.; Igawa, N.; Shamoto, S.; Maie, M.; Nagai, T.; Matsui, Y.; Stefanovich, S. Y.; Lazoryak, B. I.; Takayama-Muromachi, E. *J. Am. Chem. Soc.* **2006**, *128*, 706.
(19) Belik, A. A.; Iikubo, S.; Kodama, K.; Igawa, N.; Shamoto, S.-i.; Niitaka, S.; Azuma, M.; Shimakawa, Y.; Takano, M.; Izumi, F.; Takayama-Muromachi, E. *Chem. Mater.* **2006**, *18*, 798.
(20) Belik, A. A.; Stefanovich, S. Y.; Lazoryak, B. I.; Takayama-Muromachi, E. *Chem. Mater.* **2006**, *18*, 1964.
(21) Suchomel, M. R.; Fogg, A. M.; Allix, M.; Niu, H.; Claridge, J. B.; Rosseinsky, M. J. *Chem. Mater.* **2006**, *18*, 4987.
(22) Zylberberg, J.; Belik, A. A.; Takayama-Muromachi, E.; Ye, Z.-G. *Chem. Mater.* **2007**, *19*, 6385.
(23) Oka, K.; Azuma, M.; Hirai, S.; Belik, A. A.; Kojitani, H.; Akaogi, M.; Takano, M.; Shimakawa, Y. *Inorg. Chem.* **2009**, *48*, 2285.
(24) Belik, A. A.; Rusakov, D. A.; Furubayashi, T.; Takayama-Muromachi, E. *Chem. Mater.* **2012**, *24*, 3056.
(25) Belik, A. A. *J. Solid State Chem.* **2012**, *195*, 32.
(26) Inaguma, Y.; Katsumata, T. *Ferroelectrics* **2003**, *286*, 111.
(27) Inaguma, Y.; Miyaguchi, A.; Katsumata, T. *Mater. Res. Soc. Symp. Proc.* **2003**, *755*, 471.
(28) Tsuchiya, T.; Saito, H.; Yoshida, M.; Katsumata, T.; Ohba, T.; Inaguma, Y.; Tsurui, T.; Shikano, M. *Mater. Res. Soc. Symp. Proc.* **2007**, *988E*, 0988.
(29) Navrotsky, A. *Chem. Mater.* **1998**, *10*, 2787.
(30) Abrahams, S. C.; Reddy, J. M.; Bernstein, J. L. *J. Phys. Chem. Solids* **1966**, *27*, 997.
(31) Megaw, H. D. *Acta Crystallogr., Sect. A* **1968**, *24*, 583.
(32) Abrahams, S. C.; Bernstein, J. L. *J. Phys. Chem. Solids* **1967**, *28*, 1685.
(33) Abrahams, S. C.; Hamilton, W. C.; Sequeira, A. *J. Phys. Chem. Solids* **1967**, *28*, 1693.
(34) Kemmler, S. *Z. Anorg. Allg. Chem.* **1965**, *338*, 9.
(35) Miyake, C.; Fuji, K.; Imoto, S. *Chem. Phys. Lett.* **1979**, *61*, 124.
(36) Hinatsu, Y.; Fujino, T.; Edelstein, N. *J. Solid State Chem.* **1992**, *99*, 182.
(37) Cava, R. J.; Santoro, A.; Murphy, D. W.; Zahurak, S.; Roth, R. S. *J. Solid State Chem.* **1982**, *42*, 251.
(38) Kumada, N.; Kinomura, N. *Mater. Res. Bull.* **1990**, *25*, 881.
(39) Kumada, N.; Hosoda, S.; Muto, F.; Kinomura, N. *Inorg. Chem.* **1989**, *28*, 3592.
(40) Syono, Y.; Akimoto, S.-I.; Ishikawa, Y.; Endoh, Y. *J. Phys. Chem. Solids* **1969**, *30*, 1665.
(41) Ito, E.; Matsui, Y. *Phys. Chem. Miner.* **1979**, *4*, 265.
(42) Ko, J.; Prewitt, C. T. *Phys. Chem. Miner.* **1988**, *15*, 355.
(43) Ross, N. L.; Ko, J.; Prewitt, C. T. *Phys. Chem. Miner.* **1989**, *16*, 621.
(44) Syono, Y.; Sawamoto, H.; Akimoto, S. *Solid State Commun.* **1969**, *7*, 713.
(45) Leinenweber, K.; Utsumi, W.; Tsuchida, Y.; Yagi, T.; Kurita, K. *Phys. Chem. Miner.* **1991**, *18*, 244.
(46) Mehta, A.; Leinenweber, K.; Navrotsky, A.; Akaogi, M. *Phys. Chem. Miner.* **1994**, *21*, 207.
(47) Leinenweber, K.; Linton, J.; Navrotsky, A.; Fei, Y.; Parise, J. B. *Phys. Chem. Miner.* **1995**, *22*, 251.
(48) Hattori, T.; Matsuda, T.; Tsuchiya, T.; Nagai, T.; Yamanaka, T. *Phys. Chem. Miner.* **1999**, *26*, 212.
(49) Linton, J. A.; Fei, Y.; Navrotsky, A. *Am. Mineral.* **1997**, *82*, 639.
(50) Leinenweber, K.; Wang, Y.; Yagi, T.; Yusa, H. *Am. Mineral.* **1994**, *79*, 197.
(51) Akaogi, M.; Kojitani, H.; Yusa, H.; Yamamoto, R.; Kido, M.; Koyama, K. *Phys. Chem. Miner.* **2005**, *32*, 603.
(52) Yusa, H.; Akaogi, M.; Sata, N.; Kojitani, H.; Yamamoto, R.; Ohishi, Y. *Phys. Chem. Miner.* **2006**, *33*, 217.
(53) Funamori, N.; Yagi, T.; Miyajima, N.; Fujino, K. *Science (New York, N.Y.)* **1997**, *275*, 513.
(54) Sleight, A. W.; Prewitt, C. T. *Mater. Res. Bull.* **1970**, *5*, 207.
(55) Inaguma, Y.; Yoshida, M.; Katsumata, T. *J. Am. Chem. Soc.* **2008**, *130*, 6704.
(56) Son, J. Y.; Lee, G.; Jo, M.-H.; Kim, H.; Jang, H. M.; Shin, Y.-H. *J. Am. Chem. Soc.* **2009**, *131*, 8386.
(57) Inaguma, Y.; Yoshida, M.; Tsuchiya, T.; Aimi, A.; Tanaka, K.; Katsumata, T.; Mori, D. *J. Phys.: Conf. Ser.* **2010**, *215*, 012131.
(58) Inaguma, Y.; Sakurai, D.; Aimi, A.; Yoshida, M.; Katsumata, T.; Mori, D.; Yeon, J.; Halasyamani, P. S. *J. Solid State Chem.* **2012**, *195*, 115.
(59) Inaguma, Y.; Tanaka, K.; Tsuchiya, T.; Mori, D.; Katsumata, T.; Ohba, T.; Hiraki, K.; Takahashi, T.; Saitoh, H. *J. Am. Chem. Soc.* **2011**, *133*, 16920.
(60) Belik, A. A.; Furubayashi, T.; Matsushita, Y.; Tanaka, M.; Hishita, S.; Takayama-Muromachi, E. *Angew. Chem., Int. Ed.* **2009**, *48*, 6117.
(61) Belik, A. A.; Furubayashi, T.; Yusa, H.; Takayama-Muromachi, E. *J. Am. Chem. Soc.* **2011**, *133*, 9405.
(62) Arielly, R.; Xu, W. M.; Greenberg, E.; Rozenberg, G. K.; Pasternak, M. P.; Garbarino, G.; Clark, S.; Jeanloz, R. *Phys. Rev. B* **2011**, *84*, 094109.
(63) Shi, Y.; Guo, Y.; Wang, X.; Princep, A. J.; Khalyavin, D.; Manuel, P.; Michiue, Y.; Sato, A.; Tsuda, K.; Yu, S.; Arai, M.; Shirako, Y.; Akaogi, M.; Wang, N.; Yamaura, K.; Boothroyd, A. T. *Nat. Mater.* **2013**, *12*, 1024.
(64) Fennie, C. J. *Phys. Rev. Lett.* **2008**, *100*, 167203.
(65) Varga, T.; Kumar, A.; Vlahos, E.; Denev, S.; Park, M.; Hong, S.; Sanehira, T.; Wang, Y.; Fennie, C. J.; Streiffer, S. K.; Ke, X.; Schiffer, P.; Gopalan, V.; Mitchell, J. F. *Phys. Rev. Lett.* **2009**, *103*, 047601.
(66) Aimi, A.; Katsumata, T.; Mori, D.; Fu, D.; Itoh, M.; Kyômen, T.; Hiraki, K.; Takahashi, T.; Inaguma, Y. *Inorg. Chem.* **2011**, *50*, 6392.
(67) Nakayama, M.; Nogami, M.; Yoshida, M.; Katsumata, T.; Inaguma, Y. *Adv. Mater.* **2010**, *22*, 2579.
(68) Zhang, J.; Yao, K. L.; Liu, Z. L.; Gao, G. Y.; Sun, Z. Y.; Fan, S. W. *Phys. Chem. Chem. Phys.* **2010**, *12*, 9197.
(69) Veithen, M.; Ghosez, P. *Phys. Rev. B* **2002**, *65*, 214302.

(70) Shannon, R. D. *Acta Crystallogr., Sect. A* **1976**, *A32*, 751.
(71) Sato, H.; Endo, S.; Sugiyama, M.; Kikegawa, T.; Shimomura, O.; Kusaba, K. *Science* **1991**, *251*, 786.
(72) Kojitani, H.; Iwabuchi, T.; Kobayashi, M.; Miura, H.; Akaogi, M. *Am. Mineral.* **2011**, *96*, 1248.
(73) Kojitani, H.; Shirako, Y.; Akaogi, M. *Phys. Earth Planet. Inter.* **2007**, *165*, 127.
(74) Nishibori, E.; Takata, M.; Kato, K.; Sakata, M.; Kubota, Y.; Aoyagi, S.; Kuroiwa, Y.; Yamakata, M.; Ikeda, N. *Nuclear Instrum. Methods Phys. Res., Sect. A* **2001**, *467−468* (Part 2), 1045.
(75) Izumi, F.; Momma, K. *Solid State Phenom.* **2007**, *130*, 15.
(76) Momma, K.; Izumi, F. *J. Appl. Crystallogr.* **2011**, *44*, 1272.
(77) Kurtz, S. K.; Perry, T. T. *J. Appl. Phys.* **1968**, *39*, 3798.
(78) Kresse, G.; Furthmüller, J. *Phys. Rev. B* **1996**, *54*, 11169.
(79) Kresse, G.; Furthmüller, J. *Comput. Mater. Sci.* **1996**, *6*, 15.
(80) Perdew, J. P.; Burke, K.; Ernzerhof, M. *Phys. Rev. Lett.* **1996**, *77*, 3865.
(81) Perdew, J. P.; Ruzsinszky, A.; Csonka, G. I.; Vydrov, O. A.; Scuseria, G. E.; Constantin, L. A.; Zhou, X.; Burke, K. *Phys. Rev. Lett.* **2008**, *100*, 136406.
(82) Blöchl, P. E. *Phys. Rev. B* **1994**, *50*, 17953.
(83) Murnaghan, F. D. *Proc. Natl. Acad. Sci. U.S.A.* **1944**, *30*, 244.
(84) Togo, A.; Oba, F.; Tanaka, I. *Phys. Rev. B* **2008**, *78*, 134106.
(85) Baroni, S.; de Gironcoli, S.; Dal Corso, A.; Giannozzi, P. *Rev. Mod. Phys.* **2001**, *73*, 515.
(86) Kennedy, B. J.; Zhou, Q.; Avdeev, M. *J. Solid State Chem.* **2011**, *184*, 2987.
(87) Brown, I. D.; Shannon, R. D. *Acta Crystallogr., Sect. A* **1973**, *29*, 266.
(88) Altermatt, D.; Brown, I. D. *Acta Crystallogr., Sect. B* **1985**, *41*, 240.
(89) Brown, I. D.; Altermatt, D. *Acta Crystallogr., Sect. B* **1985**, *41*, 244.
(90) Brese, N. E.; O'Keeffe, M. *Acta Crystallogr. Sect. B* **1991**, *47*, 192.
(91) Bates, C. H.; White, W. B.; Roy, R. *Science (New York, N.Y.)* **1962**, *137*, 993.
(92) Simons, P. Y.; Dachille, F. *Acta Crystallogr.* **1967**, *23*, 334.
(93) Koopmans, H. J. A.; van de Velde, G. M. H.; Gellings, P. J. *Acta Crystallogr., Sect. C* **1983**, *39*, 1323.
(94) Hsu, R.; Maslen, E. N.; Boulay, D. d.; Ishizawa, N. *Acta Crystallogr., Sect. B* **1997**, *53*, 420.
(95) Jørgensen, C. K. *Prog. Inorg. Chem.* **1970**, *12*, 101.
(96) Eng, H. W.; Barnes, P. W.; Auer, B. M.; Woodward, P. M. *J. Solid State Chem.* **2003**, *175*, 94.
(97) Inaguma, Y.; Muronoi, T.; Sano, K.; Tsuchiya, T.; Mori, Y.; Katsumata, T.; Mori, D. *Inorg. Chem.* **2011**, *50*, 5389.
(98) Bloembergen, N. *Nonlinear Optics*, 4th ed.; World Scientific: Singapore, 1996.